PHYSICAL REVIEW B **88**, 245442 (2013)

Ab initio and cluster expansion study of surface alloys of Fe and Au on Ru(0001) and Mo(110): Importance of magnetism

Madhura Marathe,[1] Alejandro Díaz-Ortiz,[2,3] and Shobhana Narasimhan[1]
[1]*Theoretical Sciences Unit, Jawaharlal Nehru Centre for Advanced Scientific Research, Jakkur, Bangalore - 560064, India*
[2]*Synchrotron SOLEIL, l'Orme des Merisiers, St Aubin, BP48 91192 Gif-Sur-Yvette Cedex, France*
[3]*Department of Engineering Physics, McMaster University, Hamilton, Canada*

(Received 9 May 2013; revised manuscript received 30 October 2013; published 26 December 2013)

We have performed *ab initio* density functional theory calculations to study freestanding alloy monolayers of Fe and Au in centered rectangular and hexagonal geometries, as well as Fe-Au surface alloys on Ru(0001) and Mo(110) substrates. Though Fe and Au are bulk immiscible, in all four classes of systems we obtain negative formation energies. While the properties of the two classes of freestanding monolayers are roughly similar, with small differences due to the anisotropy and longer bond lengths of the centered rectangular case, the surface alloys on the two substrates behave quite differently. The formation energies on Mo(110) are markedly smaller; we trace this to the fact that magnetism contributes significantly to mixing on Ru(0001) but not on Mo(110). On Ru(0001), there is a very stable $(\sqrt{3} \times \sqrt{3})$ $FeAu_2$ phase, in agreement with experiments. By performing cluster expansion calculations, we show that ordering is not favored on Mo(110), again in accordance with experimental data.

DOI: 10.1103/PhysRevB.88.245442 PACS number(s): 68.35.bd, 68.55.Nq, 71.15.Mb

I. INTRODUCTION

The formation of thin-film alloys has gained a lot of interest after it was shown that bulk-immiscible pairs of metals can form two-dimensional mixed phases on surfaces.[1] This alloying gives rise to new structural phases and hence can lead to new material properties such as enhanced reactivity,[2–4] and high magnetic anisotropy energies. Many pairs of metals are immiscible in the bulk because of a large size mismatch, which leads to the buildup of large elastic stresses when they form a bulk alloy; this leads to the first Hume-Rothery rule governing the formation of bulk substitutional alloys.[5] However, such pairs of metals could conceivably relieve surface stress by mixing on surfaces, and this was generally believed to be the main driving force for the formation of surface alloys.[6–8]

The FeAu/Ru(0001) system seemed like an ideal system to see this mechanism at play, since, while Fe and Au are bulk immiscible, the lattice constant of Fe is 8% smaller than that of Ru, while that of Au is 7% larger. Indeed, it was experimentally found that $FeAu_2$/Ru(0001) shows a long-range-ordered surface alloy.[9] The surprising finding in this system was that it was not stress relief that was the driving force for alloy formation; instead, it was magnetism.[9] The lowest energy surface alloy structure is one in which Fe atoms surround themselves with Au atoms and thus attain a very high magnetic moment, thus lowering the exchange energy of the system. Another evidence for the dominance of magnetic interactions in this system was the finding that for a given composition, the most favored structure was always the one with the highest magnetic moment.

This prompts the question, how general are these findings? For example, would they always hold true for the same alloy constituents, regardless of the substrate? What role, if any, does the geometry of the two-dimensional lattice play? Therefore we have chosen here to compare FeAu/Ru(0001) with a very similar system—FeAu/Mo(110). Both Mo and Ru have similar electronic properties, and their bulk nearest-neighbor distances differ by only 1%. However, the geometry changes from a highly isotropic hexagonal lattice to an anisotropic centered rectangular lattice.

In order to more clearly separate out the effects of geometry versus the effects of the substrate, we have studied four classes of systems: (i) freestanding FeAu alloy monolayers on a triangular lattice, with lattice spacing equal to that of the Ru(0001) substrate; (ii) freestanding FeAu alloy monolayers on a centered rectangular lattice, with lattice spacing equal to that of the Mo(110) substrate; (iii) deposited monolayers of FeAu alloys on Ru(0001); and (iv) deposited monolayers of FeAu alloys on Mo(110). Comparison of (i) with (ii) will allow us to extract the effect of geometry alone. Comparison of (i) with (iii), or (ii) with (iv), will allow us to draw conclusions about the effects of placing the alloys on the respective substrates. Finally, comparison of (iii) and (iv) will allow us to compare the effects of the two substrates. The overall comparison of the four cases should enable us to draw inferences about the relative importance of geometry versus the chemical nature of the substrate. Examining how the magnetic moments of the alloys compare with those of the end phases allows us to discuss what role magnetism plays in driving mixing. Another way in which we can look at this question is by performing calculations in which we suppress spin polarization; we have also done this.

Both Ru(0001) and Mo(110) surfaces are well-studied surfaces, with higher surface energies than the stable Au(111) and Fe(110) surfaces.[10] Furthermore, the solubility of either Fe or Au in bulk Ru or Mo is very small. Thus diffusion of the overlayer metals into the substrate, or alloying with the substrate, is less probable, which is needed for a good surface alloy.

A. Previous work on related systems

The single-component Fe/Mo(110) system has been studied extensively, both experimentally and theoretically.[11–14] It shows a strong magnetic anisotropy, with a spin reorientation transition as a function of the Fe coverage: nanoislands and nanowires show magnetization perpendicular to the surface,[15–17] whereas thin layers have an in-plane easy axis.[18,19] This suggests that depending on whether the structure is striped or not, thin Fe-Au layers could show a variety of magnetic properties. Scanning tunneling microscopy studies done on Fe-Au nanostructures on the Mo(110) surface[20,21] have shown that there is atomic-level mixing, but no ordered structure could be identified. Furthermore, this system shows a spin reorientation as the Au coverage is varied. Therefore it will be interesting to study the structural properties of thin films of Fe-Au/Mo(110) and compare the results with these experiments.

There have been many reports on single-component Fe or Au layers deposited on the Ru(0001) surface. Fe forms two-dimensional, pseudomorphic layers on the Ru(0001) surface until a critical thickness.[22,23] For annealing temperatures >800 K, Fe and Ru are observed to form an interfacial alloy.[23] In contrast, it has been observed in experiments that even at a single monolayer coverage, Au deposited on the Ru(0001) surface has a striped pattern of dislocations forming a herringbone pattern.[24] This happens because a pseudomorphic layer would be under a large compressive stress, arising from the large atomic-size mismatch between Au and Ru. However, the difference in energy between the pseudomorphic and reconstructed structures is small. Using the two-dimensional Frenkel-Kontorova model fit to *ab initio* data, it was found to be ~ -12 meV/Å^2 (Ref. 25).

When Fe and Au are codeposited on Ru(0001), the system forms a long-range ordered, atomically mixed pseudomorphic surface alloy at compositions where the Fe concentration is about 33%.[9] However, under Fe-rich conditions, no long-range order is observed. These findings were confirmed and explained by *ab initio* density functional theory calculations.[9]

There has been an earlier theoretical study of surface alloys of Fe-Ag on the Mo(110) and Ru(0001) surfaces.[26] In this paper, possibly motivated by experimental findings,[27] the authors have restricted themselves to studying only equiatomic striped structures. They found that the alloys on Ru(0001) are more stable than those on Mo(110), at zero temperature; however, by performing Monte Carlo simulations, they found that the alloys on Ru disorder at a lower temperature than those on Mo. Given that Ag and Au have similar sizes in their bulk phases, it would be interesting to examine whether the mixing properties are similar for the two surface alloy systems.

II. COMPUTATIONAL DETAILS OF DENSITY FUNCTIONAL THEORY CALCULATIONS

We have used spin-polarized ("spin-unrestricted") density functional theory to calculate the structural properties of Fe-Au surface alloys. We have used the PWSCF code implemented in the QUANTUM ESPRESSO package,[28] which uses a plane-wave basis set. The spin-polarized version of the Kohn-Sham equations[29] are solved using a self-consistent loop, starting from an initial guess with broken spin symmetry. We have checked that when we start from different initial spin states for the starting configuration, we always converged to the same final magnetic state, giving us confidence that we have found the correct minimum in spin space. We also did a few test calculations with fixed-moment calculations and verified that we obtained the same results as with spin-unrestricted calculations. As mentioned below, in order to determine the relative importance of magnetism, a few calculations are performed, however, with spin polarization suppressed.

After extensive convergence tests, we determined that we needed kinetic energy and charge density cutoffs of 25 and 200 Ry, respectively, for calculations involving Mo, and 20 Ry and 160 Ry, respectively, for calculations involving Ru. To facilitate comparisons, the former set of cutoffs was used also for the centered rectangular freestanding monolayers and the latter set for the hexagonal freestanding monolayers. Exchange-correlation interactions were treated within the generalized gradient approximation.[30] For Brillouin zone sampling, we have used Monkhorst-Pack k-point grids[31] commensurate with a (17×17) sampling of the (1×1) surface unit cell for all centered rectangular configurations, and a (8×8) sampling for all hexagonal configurations. Note that previous authors[26] have also reported that higher plane-wave cutoffs and denser Brillouin zone sampling were required for alloys on the Mo(110) substrate than those on the Ru(0001) substrate. For faster convergence, we have used the Methfessel-Paxton smearing technique,[32] with a smearing width equal to 0.05 Ry.

We have considered supercells consisting of an overlayer of an alloy or pure Fe or pure Au, deposited on one side of either an eight-atomic-layer thick Mo slab, or a six-atomic-layer thick Ru slab. The slab thickness was determined by testing for the convergence of the surface energy. Periodic images of the slab were separated by a vacuum layer of about 16 Å thickness. To get optimized geometries, we have allowed the overlayer and three adjacent substrate layers to relax using Hellmann-Feynman forces, while the remaining layers were kept fixed at the calculated bulk nearest-neighbor spacings. We find the bulk nearest-neighbor distance to be 2.75 Å for Mo and 2.74 Å for Ru; the corresponding experimental values are 2.73 and 2.70 Å, respectively. In all cases, we have assumed the overlayer atoms occupy pseudomorphic positions at the hollow sites on the surface.

III. RESULTS AND DISCUSSION

A. *Ab initio* calculations on freestanding monolayers

We first discuss our results for freestanding monolayers of Fe-Au in centered rectangular and hexagonal geometries. In the former case, the lattice spacings are adjusted to be those of the Mo(110) surface, while in the latter they are those of the Ru(0001) surface. Experimentally, the nearest-neighbor distances of Mo and Ru are close, equal to 2.73 and 2.70 Å respectively. However, in our study, we have used our theoretically computed values, which are even closer, equal to 2.75 and 2.74 Å, respectively. In Fig. 1 we show top views of these two geometries; we see that they are very similar, with the centered rectangular structure being somewhat distorted from the sixfold symmetry of the hexagonal lattice, resulting in perceptible anisotropy. Both as a result of this distortion and because of the larger lattice constant of Mo compared to that of Ru, corresponding interatomic distances in the centered rectangular lattice are larger than in the hexagonal lattice, with the closest six atoms being at distances that are greater by a factor of 0.4% (for four atoms) and 14.6%

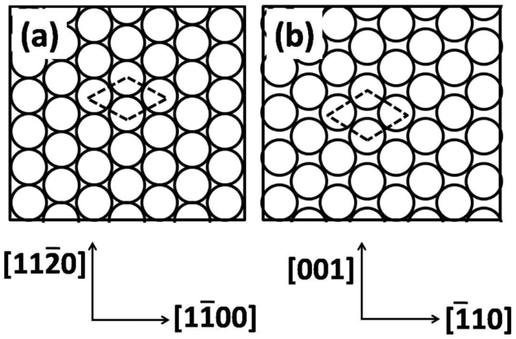

FIG. 1. Schematic top views of the (a) hexagonal and (b) centered rectangular geometries: here circles indicate lattice points, and the primitive unit cell is shown with dashed lines. We have also shown the crystallographic directions for each surface.

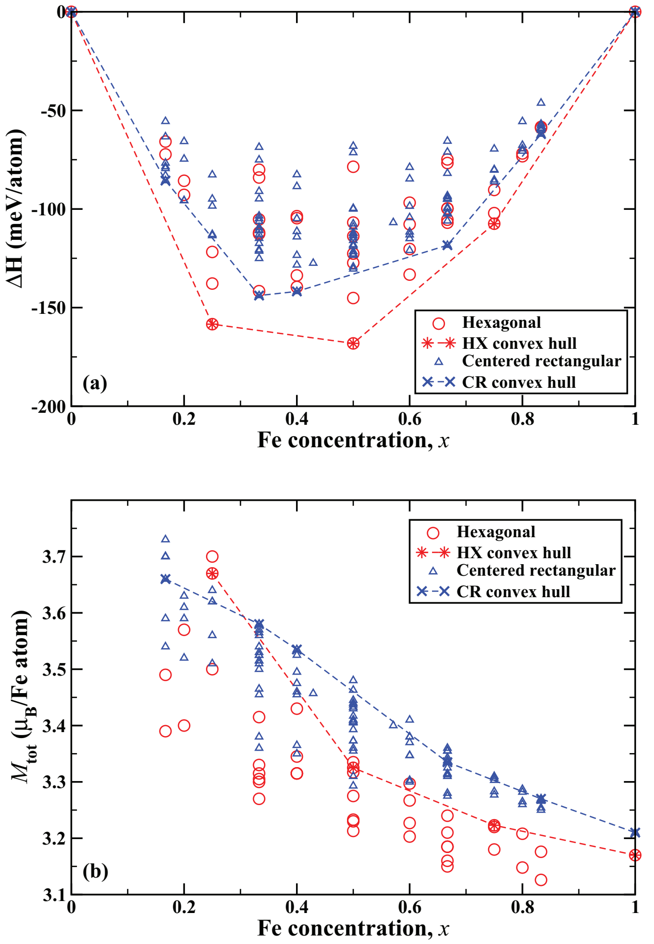

FIG. 2. (Color online) The formation energy ΔH and magnetic moments per Fe atom M_{tot} as a function of Fe concentration x for freestanding monolayers. Here circles represent the values for the hexagonal phases and triangles for the centered rectangular phases. The configurations falling on the convex hull for each of these systems are shown by stars and crosses for hexagonal (HX) and centered rectangular (CR) geometries, respectively.

(for two atoms). We wish to see what effect, if any, this expansion and anisotropy have on the mixing and magnetic properties of freestanding Fe-Au alloy monolayers in the centered rectangular and hexagonal geometries.

For the centered rectangular geometry, we have performed *ab initio* calculations on 102 symmetry-nonequivalent structures, and for the hexagonal geometry, on 43 symmetry-nonequivalent structures. For the centered rectangular geometry, all the distinct symmetry-inequivalent configurations containing up to six atoms per surface unit cell are considered, and for the hexagonal geometry, all those up to five atoms per surface unit cell and several with six atoms are considered. Information on how these configurations were generated is given in the Appendix. Note that the lower symmetry of the centered rectangular geometry results in a larger number of distinct configurations.

1. Formation energy ΔH *for freestanding monolayers*

In order to study the miscibility, we have computed whether the mixed structures are more favored as compared to the phase-segregated pure Fe or Au layers. To do this, we have calculated the formation energy of the mixed structure of $\text{Fe}_x\text{Au}_{1-x}$, defined by

$$\Delta H = E(\text{Fe}_x\text{Au}_{1-x}) - xE(\text{Fe}) - (1-x)E(\text{Au}), \quad (1)$$

where $E(A)$ is the total energy of a freestanding monolayer of A, and x is the Fe concentration. A negative value of ΔH indicates that mixing of the two components is favored.

In Fig. 2(a) we have plotted the formation energy of freestanding monolayers in the two types of geometries as a function of Fe concentration x; circles (red online) and triangles (blue online) give our results for the hexagonal and centered rectangular structures, respectively. The dashed lines on the figure connect the stable structures that lie on the convex hulls for the two classes of structures: there are five such structures for the centered rectangular lattice, and three for the hexagonal lattice. We find that the values for ΔH are quite similar for both centered rectangular and hexagonal structures, which is to be expected given the similarity between the two types of lattices. However, in general, the hexagonal structures have slightly larger $|\Delta H|$, and a lower-lying convex hull. While it is difficult to assign this to a single clear cause, we believe that a hint may be obtained by examining the surface stress. In the bulk, the Au nearest-neighbor distance is larger than that in Mo or Ru, while the distance in bulk Fe is smaller. However, the effective sizes of Au and Fe atoms in a freestanding monolayer are much smaller than in the bulk. As a result, while Fe freestanding monolayers are under tensile stress, at both centered rectangular and hexagonal geometries (as expected), only the hexagonal Au freestanding monolayer is under compressive stress, while the centered rectangular Au freestanding monolayer is also under tensile stress. Thus, in hexagonal freestanding monolayer alloys, the two single-component end members have opposite surface stress, and it becomes more favorable for the alloys to form than in the centered rectangular freestanding monolayer alloys, where the end members have surface stress of the same sign.

2. Magnetic moments for freestanding monolayers

In Fig. 2(b) we have plotted M_{tot}, the total magnetic moment (divided by the number of Fe atoms) of the two types of freestanding monolayers, as a function of x. Note that, as expected, this decreases as the Fe concentration increases for both centered rectangular and hexagonal geometries. This is because when Fe atoms have more Fe neighbors, the magnetic moment decreases due to hybridization with these neighbors. Since we find that the induced moments on Au atoms tend to align ferromagnetically with those on the Fe atoms, M_{tot} tends to follow the same trend. The magnetic moments are slightly larger for the centered rectangular geometries than for the corresponding hexagonal geometries, due to the slightly longer interatomic bond lengths in the former case.

In Fig. 2(b), points corresponding to those that lie on the convex hull in Fig. 2(a) are indicated by stars and crosses. In earlier work on FeAu/Ru(0001),[9] we had found that at a given concentration, the energetically most favored structure was always the one with the highest magnetic moment. This finding is more or less borne out in these systems too, with a couple of exceptions. One can, in general, say that a high magnetic moment tends to correlate with a low energy, i.e., a high $|\Delta H|$.

B. *Ab initio* calculations on deposited monolayers

Next, we deposit the same structures studied in the previous section, on substrates, with the centered rectangular structures deposited on a Mo(110) substrate and the hexagonal structures deposited on a Ru(0001) substrate. Having studied the freestanding monolayers beforehand allows us to more clearly separate out the effects of the substrate from the effects of the geometry. Once again, we use Eq. (1) to compute the formation energies, where, however, the phase-separated structures now refer to monolayers of either Fe or Au on the relevant substrate. Some of our results for the case of deposited monolayers on the Ru(0001) substrate have earlier been briefly presented and discussed in Ref. 9; note, however, that here the convention regarding the x and y axes is reversed to facilitate easier comparison with the centered rectangular structures.

1. ΔH for deposited monolayers

Figure 3(a) shows our results for the formation energy ΔH for deposited monolayers on the two substrates; as before, the circles (red online) refer to the hexagonal geometry [on Ru(0001)], and the triangles (blue online) to the centered rectangular geometry [on Mo(110)].

2. Comparison of ΔH for freestanding and deposited monolayers

On comparing the results in Fig. 3(a) with those in Fig. 2(a), we see that while the values of ΔH are more or less unchanged when the substrate is Ru(0001), they are reduced by about 50% for the case of deposition on Mo(110). This is our most striking result for the deposited monolayers, showing that the nature of the substrate can in some cases play a huge role in the miscibility of surface alloys, and we will analyze this in greater detail further below.

Next, if one pays attention to which structures lie on the *ab initio* convex hulls, we find that they are quite different for the freestanding and deposited monolayers, and also quite different in nature for the hexagonal and centered rectangular deposited monolayers. Figure 4 shows some of the structures that lie on the *ab initio* convex hulls for the freestanding and deposited monolayers. In general, the low-lying structures for the hexagonal deposited monolayers tend to feature isolated atoms of one type surrounded by atoms of the other type, while the energetically most favored structures for centered rectangular deposited monolayers are almost always stripes oriented along the $[\bar{1}10]$ or x direction. This difference in the two types of favored structures has two origins: the greater importance of magnetism in the alloys on Ru(0001) as opposed to Mo(110) (this point is elaborated on further below), as well as the anisotropic nature of the bcc(110) surface as opposed to the isotropic hcp (0001) surface.

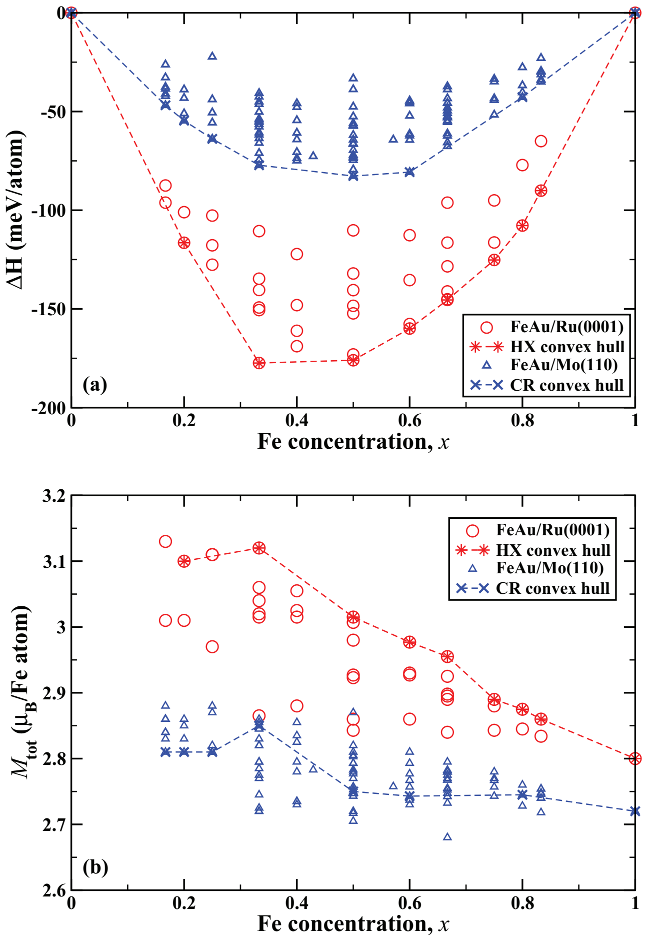

FIG. 3. (Color online) The formation energy ΔH and magnetic moments per Fe atom M_{tot} as function of Fe concentration x for deposited monolayers. Here circles represent the values for the hexagonal phases and triangles for the centered rectangular phases. The configurations falling on the convex hull for each of these systems are shown by stars and crosses for hexagonal (HX) and centered rectangular (CR) geometries, respectively.

3. ΔH for striped structures for the centered rectangular geometry

In the earlier mentioned studies on Fe-Ag alloys,[26] the authors restricted themselves to equiatomic striped structures, whereas we have considered all possible structures with small unit cells. In their work, the authors looked at how the

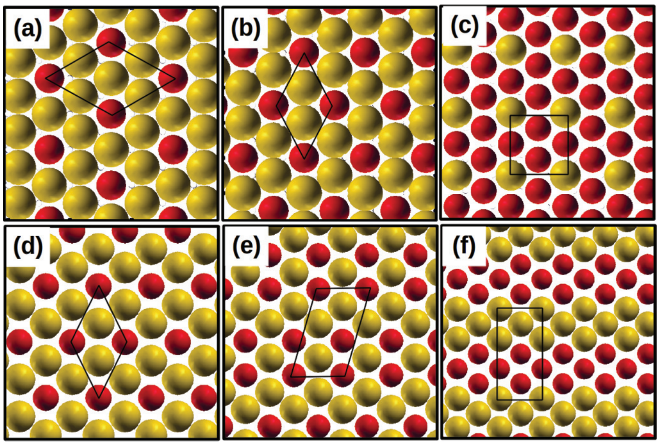

FIG. 4. (Color online) Top views of example structures lying on the hexagonal (top row) and centered rectangular (bottom row) convex hulls. We have shown the following configurations: (a) $FeAu_3$ with a (2×2) unit cell for hexagonal freestanding monolayer; (b) $FeAu_2$ with a $(\sqrt{3} \times \sqrt{3})$ unit cell for hexagonal deposited monolayer; (c) Fe_3Au with a $(\sqrt{3} \times 2)$ unit cell for a hexagonal deposited monolayer; (d) $FeAu_2$ with a $(2\sqrt{2}/\sqrt{3} \times \sqrt{5}/\sqrt{3})$ unit cell for both a centered rectangular freestanding and deposited monolayer; (e) Fe_2Au_3 with $(2\sqrt{2}/\sqrt{3} \times 3)$ for centered rectangular freestanding monolayers; and (f) Fe_3Au_3 with a $(2\sqrt{2}/\sqrt{3} \times 6/\sqrt{3})$ unit cell for a centered rectangular deposited monolayer. Fe and Au atoms are shown by dark (red online) and bright (yellow online) spheres, and the solid lines show the unit cell. Note that the most stable structures at $x = 0.33$ for the deposited monolayer phases in (b) hexagonal and (d) centered rectangular geometries are analogous structures, that is, the latter can be obtained by a slight distortion of the former.

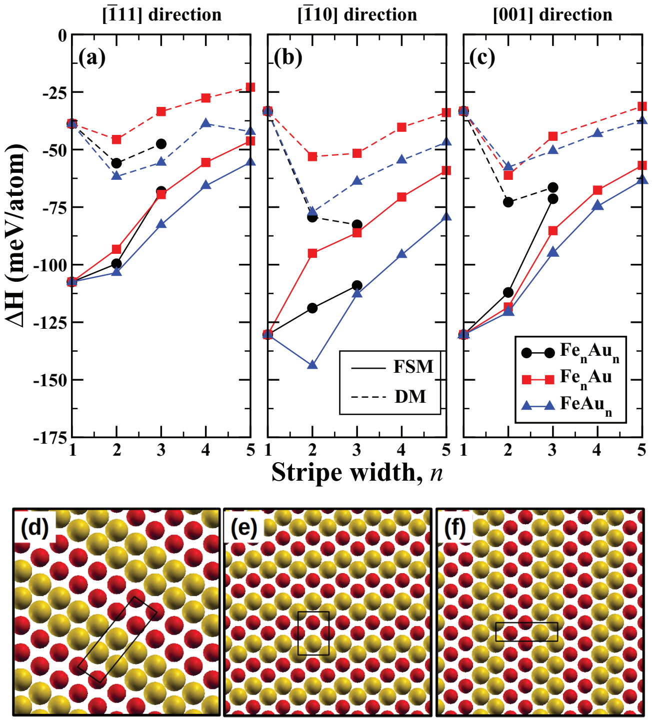

FIG. 5. (Color online) The formation energy ΔH as a function of stripe width n for striped structures, for the centered rectangular geometry, along (a) [$\bar{1}$11], (b) [$\bar{1}$10], and (c) [001] directions. Here we have considered three kinds of stripes Fe_nAu_n (black circles), Fe_nAu (red squares), and $FeAu_n$ (blue triangles). Solid lines give results for the freestanding configurations (FSM) and dashed lines for deposited monolayers (DM). We have also shown top views of Fe_2Au_2 in unit cells (d) (4×1), (e) $(2\sqrt{2}/\sqrt{3} \times 4/\sqrt{3})$, and (f) $(4\sqrt{2}/\sqrt{3} \times 2/\sqrt{3})$ as typical examples of striped structures along [$\bar{1}$11], [$\bar{1}$10], and [001] directions, respectively. Here dark (red) and bright (yellow) spheres indicate Fe and Au atoms, respectively, and the unit cell is shown by solid lines.

formation energy of the striped structures varied with the stripe periodicity. We can also do this by extracting the data for the striped structures from our pool of structures. We consider three kinds of stripes: Fe_nAu_n, $FeAu_n$, and Fe_nAu, where n is the stripe width or the number of atomic rows. Furthermore, these stripes can be oriented along three high-symmetry directions, [$\bar{1}$11], [$\bar{1}$10], and [001]. Sample structures of these various kinds of stripes are shown in Figs. 5(d)–5(f), and our results for ΔH versus n, for the centered rectangular deposited monolayers and centered rectangular freestanding monolayers are shown in Figs. 5(a)–5(c). For the Fe-Ag system, the authors of the previous study[26] had found that rather long-period stripes were favored, whereas in our study, we find that for nearly all the kinds of stripes we consider, the most energetically favored structure has a rather low period. This reflects the fact that Fe-Au alloys are more miscible than Fe-Ag alloys, as we have noted before,[33,34] since a longer-period striped structure more closely resembles a phase-segregated structure, having a rather low proportion of bonds between unlike atoms. Another difference between our results and theirs is that their lowest-energy striped structures are oriented along [001], while ours are oriented along [$\bar{1}$10].

4. *Magnetic properties of deposited monolayers*

We argue that the key to the differing behavior of the two classes of deposited systems, viz., FeAu/Mo(110) and FeAu/Ru(0001), is provided by examining their magnetic properties. Figure 3(b) shows how M_{tot} changes as a function of Fe concentration x for the alloys on Mo (blue triangles) and on Ru (red circles). Quite clearly, the moments are significantly larger on the Ru(0001) substrate than on the Mo(110) substrate. More crucially, the moments do not change much as a function of x in the latter case, while they do so in the former case. It is this latter observation that can explain why $|\Delta H|$ is reduced so markedly upon deposition on Mo, but not upon deposition on Ru. As an example, if one considers the points at or close to the convex hull at $x = 0.5$, upon mixing, M_{tot} increases by $\sim 0.15\ \mu_B$ for the hexagonal freestanding monolayer, by $\sim 0.25\ \mu_B$ for the centered rectangular freestanding monolayer, by $\sim 0.3\ \mu_B$ for the hexagonal deposited monolayer, and by $\sim 0.01\ \mu_B$ for the centered rectangular deposited monolayer. It is strikingly obvious that the increase in magnetic moment is lower, by an order of magnitude, in the last of these four cases than it is in the first three cases. So for the first three cases, magnetism provides a strong inducement for the alloys to mix:[9,35] when the alloy forms, the magnetic moments increase significantly, and thus exchange interactions significantly lower the energy of the resulting system, resulting in larger values of $|\Delta H|$. However, this effect is absent in the case of deposited monolayers on

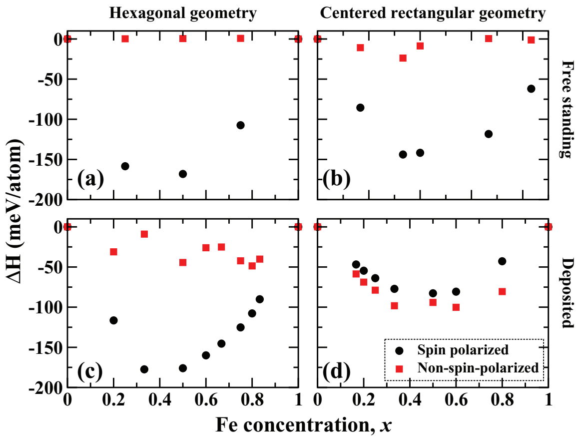

FIG. 6. (Color online) Comparison of formation energies obtained by performing spin-polarized (SP) and non-spin-polarized (NSP) calculations. The formation energy ΔH is plotted as a function of the Fe concentration x. Here we have restricted ourselves to those configurations which fall on the SP convex hulls. (a) and (b) are for freestanding monolayers, and (c) and (d) for deposited monolayers on Ru(0001) and Mo(110), respectively.

the Mo(110) substrate, and thus this contribution to ΔH is absent, resulting in the marked lowering of $|\Delta H|$. Also note that for the centered rectangular deposited monolayer system (in marked contrast to the other three systems), the highest magnetic moments do not at all correspond to the lowest $|\Delta H|$ values [see the position of the blue dashed line in Fig. 3(b)].

We note that the same effect may be present in the results of previous authors in Fe-Ag alloys on Ru(0001) and Mo(110) substrates,[26] with their reported values of $|\Delta H|$ being significantly larger on the Ru substrate than on the Mo substrate. While these authors do not discuss magnetism, or present results on magnetic moments, we speculate that a similar effect might be operating in their systems, too.

Another and more direct way of checking whether the mixing is significantly affected by the presence of magnetism is to test what happens when magnetic effects are suppressed, by performing non-spin-polarized calculations. We have done this for the configurations falling on the spin-polarized convex hulls for the four classes of systems considered here. We have compared the formation energies for the non-spin-polarized systems with the corresponding spin-polarized systems, as shown in Fig. 6. Note that the non-spin-polarized formation energies are calculated with respect to the non-spin-polarized end points. The results are strikingly different for FeAu/Mo(110), compared to the other three classes of systems. For FeAu/Mo(110), the value of $|\Delta H|$ does not change appreciably on suppressing spin polarization, though it increases very slightly. In marked contrast, for the remaining three classes of systems $|\Delta H|$ reduces significantly on suppressing the spin polarization. These results provide unambiguous evidence that exchange interactions contribute significantly to $|\Delta H|$ for the freestanding monolayers and for FeAu/Ru(0001), but not for FeAu/Mo(110), thus bolstering the conclusions drawn earlier from the results for the changes in magnetic moments as a function of x.

TABLE I. Magnetic moments for representative systems consisting of Fe_xAu_{1-x} alloys deposited on either a Ru(0001) or Mo(110) substrate. We have tabulated here the local magnetic moment on Fe atoms, and the induced moments on the Au atoms and the substrate atoms in the topmost layer. Here we have given values only for a few representative systems at different Fe concentrations x, and we have selected corresponding structures for the hexagonal (labeled by HX) and centered rectangular (labeled by CR) cases. The last column gives the total magnetic moment, per Fe atom, for the structure.

x		Magnetic moments (μ_B)			M_{tot} (μ_B
Unit cell	Geometry	Fe	Au	Ru/Mo	per Fe atom)
0.25 (2 × 2)	CR	3.10	−0.008	−0.035	2.88
	HX	3.08	0.015	0.050	3.11
0.50 (2 × 1)	CR	3.03	−0.028	−0.076	2.82
	HX	3.04	−0.009	0.058	2.98
0.75 (2 × 2)	CR	2.97	−0.064	−0.112	2.77
	HX	2.99	−0.055	0.025	2.88

It remains to understand just why the magnetic behavior on the two substrates is different. For this, we project the wave functions to get contributions to charges and magnetic moments from individual atoms. Due to the difficulty of presenting the large amount of data thus obtained, we choose to present data from just a small number of representative systems in Table I. In this table, we show, for a few structures at different Fe concentrations x, the contribution to the magnetic moment from the Fe atoms, the Au atoms, and the Ru/Mo atoms in the topmost substrate layer. In every case, we have chosen corresponding structures for the hexagonal and centered rectangular cases such that the latter can be obtained by a distortion of the former. On examining the values in the table, we find that the values of the magnetic moments on the Fe atoms are very similar in the hexagonal and centered rectangular cases, with the Fe moment increasing as x decreases. The difference is seen in the moments on the Au atoms, and, most markedly, the substrate atoms. The atoms in the topmost Ru layer are polarized ferromagnetically with respect to the Fe atoms, whereas those in the topmost Mo layer are polarized antiferromagnetically. Thus the net effect in the case of the Ru substrate is a marked increase in M_{tot} as x is decreased, whereas in the case of the Mo system, there is almost no change in M_{tot}. This, in turn, as we have discussed above, results in the differing miscibility properties on the two substrates.

C. Comparison with experiment

Finally, we compare our results on the structures of stable phases of the deposited monolayers to the available experimental data. For the case of FeAu/Ru(0001), our database of *ab initio* results suffices to explain all aspects of experimental results, as we have shown before.[9] To summarize briefly, combined scanning tunneling microscopy and low-energy electron diffraction experiments show that under Au-rich conditions, the most stable structure is a $(\sqrt{3} \times \sqrt{3})$ $FeAu_2$ structure with long-range order, which is indeed the most stable structure on our convex hull (see Figs. 3 and 4); there are no nearby competing phases, neither at the same x, nor at nearby x. In contrast, for Fe-rich conditions, experiments show that there is short-range order but no long-range order, this can be explained by the number of competing phases in the right-hand side of Fig. 3(a) for Fe-Au/Ru(0001), with five points lying on the convex hull, and also several points lying close to the convex hull. Given the fact that our *ab initio* results can essentially explain all the main features of the experimental results, we see no need to extend the study for this system at present.

The situation for Fe-Au/Mo(110) is not so clear. Our *ab initio* results (admittedly with relatively small unit cells) yield a convex hull with a few stable phases [see Fig. 3(a)], while experiments[20,21] show homogeneous mixing with scanning tunneling microscopy, while observing no superstructures with low-energy electron diffraction, suggesting the absence of any ordered phases. However, based on our *ab initio* calculations, we might have expected to see a $(2\sqrt{2}/\sqrt{3} \times 3)$ structure at $x = 0.60$. In order to examine this issue further, we decided to explore the Fe-Au/Mo(110) system in greater detail by making use of the cluster expansion technique. Moreover, to enable a comparison with the corresponding deposited monolayers case, this study was also performed for the corresponding centered rectangular freestanding monolayer systems. These results are presented in the next section.

D. Cluster expansion calculations on centered rectangular configurations

1. Introduction to the cluster expansion method

The cluster expansion method is a lattice-model-based technique.[36,37] This method casts the alloy energetics into a generalized Ising model with many-body interactions. In other words, the cluster expansion gives a coarse model of the alloy energetics where all but the configurational degrees of freedom (e.g., electronic, elastic, etc.) have been subsumed into the effective cluster interactions. When used along first-principles methods, the cluster expansion produces an effective model for the relevant (configurational) degrees of freedom. There exist some other ways of mapping the total energy landscape on simplified electronic Hamiltonians such as tight binding models,[38,39] effective pair potentials,[40,41] etc.

In the cluster expansion method, a configuration σ for an A-B alloy is defined in terms of the occupation of each lattice site by an atom A or B:

$$\sigma \equiv \{S_i\}, \qquad i = 1,2,\ldots,N, \tag{2}$$

where N is the number of lattice points in the system, and the occupation variable $S_i = +1$ or -1, depending on whether a site i is occupied by an atom of type A or B, respectively. Then, the energy of an alloy in a configuration σ is defined in terms of the occupation variables as

$$E_{\mathrm{CE}}(\sigma) = \sum_{\alpha} V_\alpha \phi_\alpha, \tag{3}$$

where $\phi_\alpha = \langle S_1 S_2 \cdots S_\alpha \rangle$ are the well-known multisite correlation functions associated to a cluster (of lattice sites) α with k sites, that is, the configurational average of the occupation variables describing cluster α.[42] The V_α's are the so-called effective cluster interactions, which are concentration independent. The notation in Eq. (3) is synthetic, underscoring a very important and practical aspect of the cluster expansion: rigorously, the determination of an infinite set of parameters (the V_α's) needs an infinite number of energy configurations. The power of the cluster expansion is based on the notion that the configurational degrees of freedom and the crystal structures of metals and alloys are strongly correlated and thus amenable to be described by only a small set of parameters. The problem is that concentration-independent interactions do not follow any compactness or short-rangedness criteria, and special schemes have been developed to find the relevant parameters in the expansions.[43] Once determined, the effective cluster interactions (V_α's) can be used to describe the energetics of alloys with larger unit cells, including disordered alloys. This makes the cluster expansion technique extremely useful, when used in combination with density functional theory calculations, to study larger unit cells. In this paper, we have chosen the variational implementation to the cluster expansion to determine the few relevant terms in Eq. (3).[44]

The *ab initio* results described above constitute the density functional theory database to which we will fit in order to find the optimal pool of clusters that gives a satisfactory cluster expansion. We have fit the formation energy of alloys to ΔH using the cross-validation algorithm.[44–46] In this method, we consider a large cluster pool containing N_c clusters (N_c is less than the number of structures N_s in the input data set) and then reduce the number of clusters such that fitting and prediction errors are minimized. In order to get the prediction error, we have employed the "leave-one-out" algorithm in which one structure is excluded from the original data set and fitting is done to the remaining $N_s - 1$ structures; the excluded structure is used to compute how good the fit is. The prediction error or the cross-validation score is defined by

$$\delta_{CV}^2 = \frac{1}{N_s} \sum_{\{p\}} [E_{AI}(p) - E_{CE}(p)]^2, \tag{4}$$

where $E_{AI}(p)$ denotes the *ab initio* formation energy of the configuration p and the sum is taken over all the configurations $\{p\}$ excluded from the original data. To ensure good convergence, we have considered five to ten different starting pools, including up to ten smallest pairs, triplets, four-point, five-point, and six-point cluster figures. A well-converged solution is one where there is reasonable agreement between the values of ΔH calculated using both density functional theory and the cluster expansion, and where removal of any cluster from the solution leads to a large increase in the fitting and prediction errors.[43]

2. Results using the cluster expansion method

In Fig. 7, we have shown how the fitting and cross-validation errors vary with the number of clusters retained, for both the freestanding monolayers and deposited monolayers. In the circled region, we see that (i) the error is acceptably small, less than 5 meV/atom, and (ii) if we were to eliminate some cluster figures, the result would be a large increase in error;[47] this is the region in which we decide to truncate the expansion. For the converged cluster expansion chosen by us, the square-root error considering all input structures

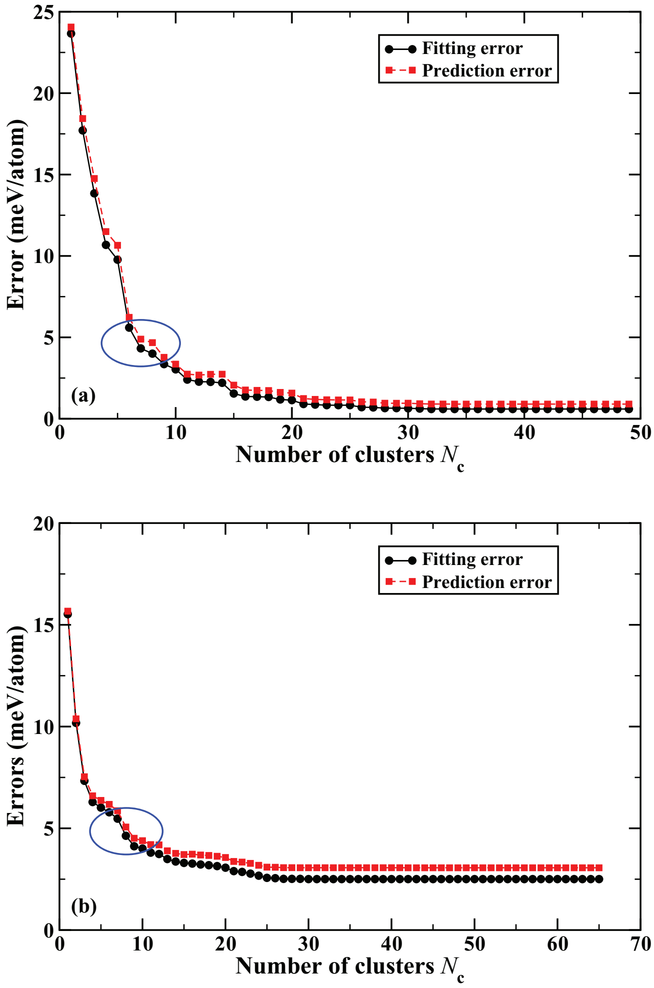

FIG. 7. (Color online) Fitting and prediction errors for (a) freestanding and (b) deposited monolayers. Here we have plotted a typical example of the variation of the fitting (black circles) and prediction errors (red squares), as the number of clusters N_c in the cluster pool is reduced. When the pool size is large, removal of a cluster does not affect errors significantly; however, as the pool size decreases, errors start to increase. We have circled the regions where there is a sudden increase in both types of errors.

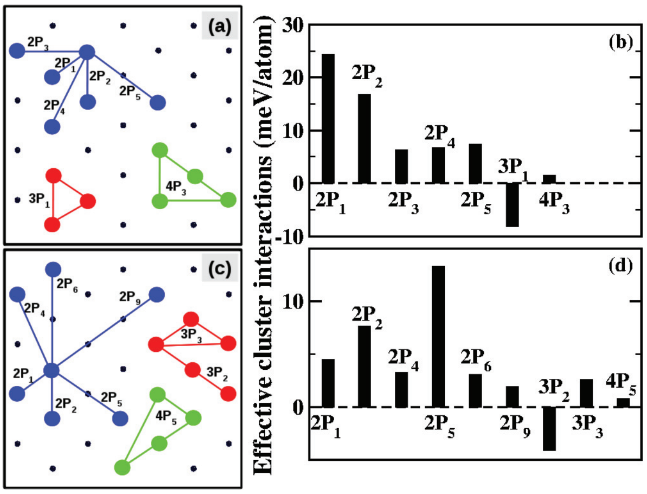

FIG. 8. (Color online) The optimal cluster sets and the corresponding effective cluster interactions for centered rectangular geometries. The top two panels show the results for the freestanding monolayers, and the bottom two panels for deposited monolayers. The effective cluster interactions are in units of meV/atom. See the text for the convention used in labeling the clusters.

averages out to 4.52 meV/atom for freestanding monolayers and 4.12 meV/atom for deposited monolayers.

In Figs. 8(a) and 8(c) we have shown the optimal sets of cluster figures required to get a good fit of the *ab initio* data for the centered rectangular freestanding monolayers and the centered rectangular deposited monolayers, respectively. In Figs. 8(b) and 8(d), we have plotted bar charts indicating the values of the corresponding effective cluster interactions. Each cluster is denoted by the nomenclature kP_l, where k is the number of lattice points in the cluster and "l" is an integer indicating the "size" of that cluster, such that $l = 1$ for the shortest possible cluster of that type. Thus, for example, $2P_1$ is the shortest possible two-body cluster connecting nearest-neighbor sites on the lattice. We see that we have seven cluster figures for the freestanding monolayers, and nine for the deposited monolayers. Also, the clusters for the deposited monolayers tend to have longer lengths, indicating that long-range interactions are more important here, possibly due to the presence of substrate-mediated elastic interactions. A positive value of an effective cluster interaction favors occupation by unlike atoms, while a negative value favors occupation by like atoms.

In Fig. 9 we have once again plotted our *ab initio* results for ΔH (see the open circles), together with the results obtained

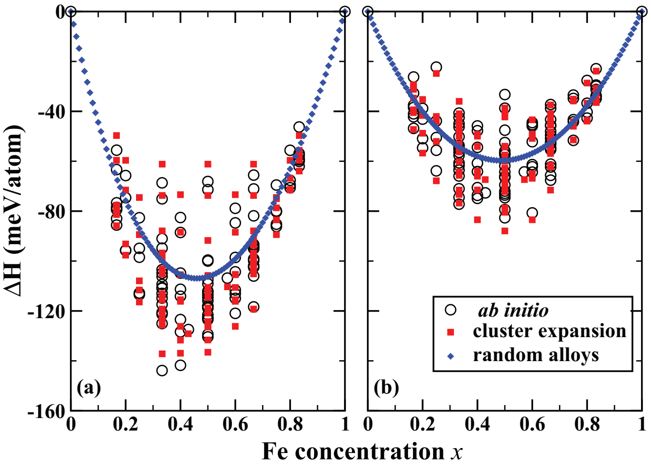

FIG. 9. (Color online) Comparing the *ab initio* and cluster expansion calculated ΔH as a function of Fe concentration x, for centered rectangular geometries, for (a) freestanding and (b) deposited monolayers. We have plotted here the formation energies obtained by density functional theory (open circles) and cluster expansion (filled squares). The cluster expansion calculated values are obtained by using the clusters shown in Fig. 8 and the corresponding effective cluster interactions. Note that the values from the two methods compare well with each other. We have also shown the formation energies for random alloys (diamonds) as calculated from the cluster expansion method.

from the cluster expansion (filled squares, red online). We can see that the difference between the two sets of results is acceptably small. We have also plotted (diamonds, blue online) the results for a random alloy, as computed using the cluster expansion. The random alloy at a concentration x is defined such that its average of occupation variables is given by

$$\phi_\alpha^{\text{random}} = (2x-1)^k \tag{5}$$

for a cluster figure α having k lattice sites. Note that for both freestanding monolayers and deposited monolayers, we find that ΔH is negative for random alloys, implying that they are stable. However, at all x, the $|\Delta H|$ values are less for random alloys as compared to the ordered ground-state structures obtained from density functional theory, which implies that ordering is more favored than random alloys.

We are now in a position to check whether there are ordered structures with larger unit cells than those considered in our *ab initio* calculations, or whether the clear-cut convex hulls obtained by us disappear on considering larger unit cells. To do this, we use Eq. (3) to compute the energies of all distinct alloy configurations containing up to 20 atoms per surface unit cell. We note that by doing this, we have hugely increased the number of configurations we are studying, which now becomes more than a million. We could never hope to compute the energies of such a large number of structures using *ab initio* calculations alone, and thus the cluster expansion becomes essential to carry out this part of our ground-state search. The distinct configurations were obtained using the enumeration code developed by Hart and Forcade;[48] the code is based on a group theoretic approach. We choose to restrict ourselves to a maximum unit cell size of 20 surface atoms, because this is equivalent to a length scale of about 40–50 Å and in actual experiments, at this scale already defects come into the picture.

The formation energies calculated using the optimized cluster expansion Hamiltonian are plotted in Fig. 10 for the freestanding monolayers [panel (a)] and for the deposited monolayers [panel (b)]. For all the configurations considered here, we find that the ΔH values are negative, implying that mixing is favored whether the alloy monolayer is supported or not.

For both the freestanding and deposited monolayers, there is basically no jagged convex hull now; instead, there is a smooth curve. Thus we can now understand the absence of any ordered structures in the experiments on Fe-Au/Mo(110).[20,21] If we were to closely examine the lowest-lying phases at various values of x, we find that they usually tend to be striped structures, with the stripes oriented along the $[\bar{1}10]$ direction. This is in contrast with the Fe-Ag/Mo(110) system, in which both experiments[27] and calculations[26] found stable structures with stripes along the perpendicular [001] direction. The preference for stripes oriented along the $[\bar{1}10]$ or x direction, rather than the [001] or y direction for our deposited monolayer systems, can be traced back to the absence of a $2P_3$ two-body cluster in our optimal pool for the deposited monolayers, and a positive value for the effective cluster interaction corresponding to $3P_3$, as a result of which like neighbors are favored along the x direction. We do not believe that the preference for stripes along x rather than y is an artefact of a poorly converged cluster expansion, since the same preference can also be seen in our *ab initio* density functional theory results [see Fig. 4(f)]. However, we note that this energetic preference is small, and as already noted, we do not have a clearly identifiable convex hull with well-defined stable phases.

IV. SUMMARY AND CONCLUSIONS

To summarize, we have studied Fe-Au alloys in four classes of systems: in centered-rectangular and hexagonal geometries, and freestanding and deposited on Mo(110) and Ru(0001) substrates. If one were to separate out the effect of geometry alone, by considering freestanding monolayers, then it is not that marked, though structures featuring isolated atoms of one species surrounded by atoms of the other species are favored on the isotropic hexagonal lattice, while striped structures are also favored on the anisotropic centered rectangular lattice. For freestanding monolayers, the formation energy of alloys is comparable in the two geometries.

However, deposition on a substrate has a marked effect on formation energies of alloys. When the Fe-Au monolayers are deposited on Ru(0001), the formation energies remain more or less unaltered, but on Mo(110) they are approximately halved. This is because magnetism plays an important role in the mixing properties on FeAu/Ru(0001) (as we have pointed out before[9]), as it does in mixing in the freestanding monolayers; however, this effect is basically absent on FeAu/Mo(110). This, in turn, can be traced back to the fact that in the latter system, Mo atoms in the substrate tend to be spin polarized opposite to the Fe atoms in the overlayer, and any gain in magnetic moment of Fe atoms on alloying is basically offset by the opposite spin polarization of the Mo atoms. Thus the lowering

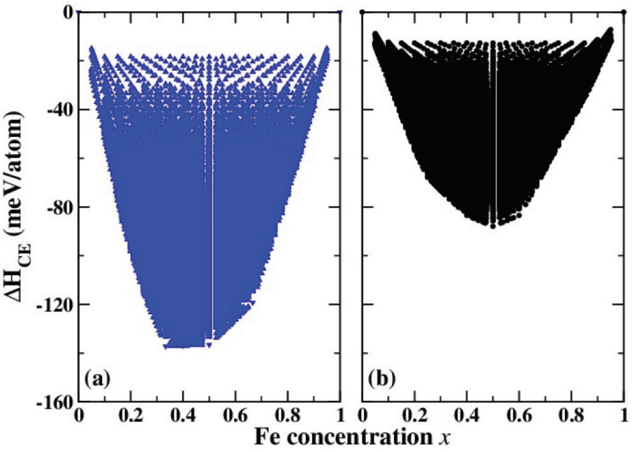

FIG. 10. (Color online) The formation energy of alloy configurations calculated using the cluster expansion Hamiltonian ΔH_{CE} versus Fe concentration x for centered rectangular geometries for (a) freestanding monolayers and (b) deposited monolayers on Mo(110). The formation energy of all alloy configurations containing up to 20 atoms per surface unit cell is plotted here. For a comparison between *ab initio* results and corresponding CE results, the reader is referred to Fig. 9.

of exchange energy does not provide a significant driving force for mixing in this system.

In this study, we have presented four kinds of evidence to show that magnetism plays a role in the differing behavior of FeAu/Ru(0001) and FeAu/Mo(110):

(i) Figure 6, i.e., the comparison between the spin-polarized and non-spin-polarized curves of ΔH vs x for the two systems. This shows that for FeAu/Ru(0001), but not for FeAu/Mo(110), a large contribution to the negative formation energy comes from exchange interactions.

(ii) The differing slopes of the curves of magnetic moment vs x [see Fig. 3(b)] for the two classes of systems. This shows that for FeAu/Ru(0001), but not for FeAu/Mo(110), the system can raise its magnetic moment (and thus lower its exchange energy) by alloy formation.

(iii) The fact that the rule "the lowest energy structure at a given x corresponds to the highest magnetic moment at that x" is obeyed by FeAu/Ru(0001) but not by FeAu/Mo(110). This shows that magnetism plays an important role in the former but not in the latter.

(iv) The (hand-waving) argument that the preferred structures for FeAu/Ru(0001) feature isolated Fe atoms surrounded by Au atoms (wherein Fe atoms can maximize their magnetic moment), whereas the preferred structures for FeAu/Mo(110) feature stripes of Fe atoms, wherein Fe atoms, having hybridized with more Fe neighbors, have lower moments.

In an earlier study, we had compared the alloying of several pairs of metals on Ru and Rh substrates.[49] At that time we had reached the tentative conclusion that the substrate, while important for magnetic properties, is not very important in determining miscibility. Our results here show that we now have to revise that inference, precisely because one cannot separate out miscibility and magnetism, as we have shown above: the two are intimately connected, and magnetism can have a big impact on miscibility. In our earlier study, we had missed this effect because both Ru and Rh substrates tend to get spin polarized in the same direction as the Fe atoms, and thus behave in the same way.

We have also shown that the interatomic interactions, and thus the most favored structures, are influenced by the presence of the substrate. In agreement with experiment, FeAu/Ru(0001) has a clearly identifiable $(\sqrt{3} \times \sqrt{3})$ structure, while FeAu/Mo(110) has a smoothly curved convex hull and thus no structures exhibiting long-range order.

ACKNOWLEDGMENTS

We would like to acknowledge the Texas Advanced Computing Center of the University of Texas, Austin, for computational facilities. We thank M. S. Narasimhan for drawing our attention to Ref. 50.

APPENDIX: FORMULA FOR GENERATING DISTINCT UNIT CELLS

This Appendix describes the procedure utilized to generate all possible distinct two-dimensional configurations of a given size and geometry, used for our density functional theory calculations.

We first generate all nonequivalent unit cells containing n_a surface atoms using the following procedure:[50]

Let $\bar{a}_1$ and $\bar{a}_2$ be the basis vectors for the lattice.

Consider first the case in which n_a is a prime number, then let $n_a = p$. The total number of possible unit cells is equal to $(p+1)$ and the unit cells are defined by basis cell vectors

$$\begin{aligned}&(p\bar{a}_1,\bar{a}_2)\\&(\bar{a}_1 + 0 \times \bar{a}_2, p\bar{a}_2)\\&(\bar{a}_1 + 1 \times \bar{a}_2, p\bar{a}_2)\\&\quad\vdots\\&[\bar{a}_1 + (p-1) \times \bar{a}_2, p\bar{a}_2].\end{aligned} \tag{A1}$$

Next we consider the case where n_a is not a prime number. We then consider all possible values of whole numbers b, c, and d such that $b \times d = n_a$, $b \geqslant 1$, and $0 \leqslant c < d$. The basis vectors for all possible unit cells containing n_a surface atoms are then given by

$$(b\bar{a}_1 + c\bar{a}_2, d\bar{a}_2). \tag{A2}$$

We have used these formulas to obtain all the smallest unit cells ($n_a \leqslant 6$) for the hexagonal and the centered-rectangular geometries.

Once the unit cell has been obtained, then for each value of x, the problem of obtaining the distinct configurations is reduced to the simple problem of the number of inequivalent ways of distributing xn_a Fe atoms and $(1-x)n_a$ Au atoms among n_a sites.

---

[1] L. P. Nielsen, F. Besenbacher, I. Stensgaard, E. Lægsgaard, C. Engdahl, P. Stoltze, K. W. Jacobsen and J. K. Nørskov, Phys. Rev. Lett. **71**, 754 (1993).

[2] D. I. Enache, J. K. Edwards, P. Landon, B. Solsona-Espriu, A. F. Carley, A. A. Herzing, M. Watanabe, C. J. Kiely, D. W. Knight, and G. J. Hutchings, Science **311**, 362 (2006).

[3] A. F. Lee, S. F. J. Hackett, G. J. Hutchings, S. Lizzit, J. Naughton, and K. Wilson, Catal. Today **145**, 251 (2009).

[4] A. Gros, J. Phys.: Condens. Matter **21**, 084205 (2009).

[5] W. Hume-Rothery and H. M. Powell, Z. Kristallogr. **91**, 23 (1935).

[6] J. Tersoff, Phys. Rev. Lett. **74**, 434 (1995).

[7] B. Sadigh, M. Asta, V. Ozoliņš, A. K. Schmid, N. C. Bartelt, A. A. Quong, and R. Q. Hwang, Phys. Rev. Lett **83**, 1379 (1999).

[8] J. Yuhara, M. Schmid, and P. Varga, Phys. Rev. B **67**, 195407 (2003).

[9] S. Mehendale, Y. Girard, V. Repain, C. Chacon, J. Lagoute, S. Rousset, M. Marathe, and S. Narasimhan, Phys. Rev. Lett. **105**, 056101 (2010).

[10] L. Vitos, A. V. Ruban, H. L. Skriver, and J. Kollar, Surf. Sci. Lett. **411**, 186 (1998).

[11] M. Tikhov and E. Bauer, Surf. Sci. Lett. **232**, 73 (1990).

[12] J. Malzbender, M. Przybylski, J. Giergiel, and J. Kirschner, Surf. Sci. Lett. **414**, 187 (1998).

[13] S. Murphy, D. Mac Mathúna, G. Mariotto, and I. V. Shvets, Phys. Rev. B **66**, 195417 (2002).

[14] X. Qian, F. Wagner, M. Petersen, and W. Hübner, J. Magn. Magn. Mater. **213**, 12 (2000).

[15] M. Bode, O. Pietzsch, A. Kubetzka, and R. Wiesendanger, Phys. Rev. Lett. **92**, 067201 (2004).

[16] J. Prokop, A. Kukunin, and H. J. Elmers, Phys. Rev. Lett. **95**, 187202 (2005).

[17] J. Prokop, A. Kukunin, and H. J. Elmers, Phys. Rev. B **73**, 014428 (2006).

[18] X. Qian and W. Hübner, Phys. Rev. B **64**, 092402 (2001).

[19] V. Usov, J. Murphy, and I. V. Shvets, J. Magn. Magn. Mater. **283**, 357 (2004).

[20] A. Kukunin, J. Prokop, and H. J. Elmers, Acta Phys. Pol. A **109**, 371 (2006).

[21] J. Prokop, A. Kukunin, and H. J. Elmers, Phys. Rev. B **75**, 144423 (2007).

[22] S. Andrieu, M. Piecuch, and J. F. Bobo, Phys. Rev. B **46**, 4909 (1992).

[23] J. Kolaczkiewicz and E. Bauer, Surf. Sci. Lett. **423**, 292 (1999).

[24] W. L. Ling, J. C. Hamilton, K. Thürmer, G. E. Thayer, J. de la Figuera, R. Q. Hwang, C. B. Carter, N. C. Bartelt, and K. F. McCarty, Surf. Sci. Lett. **600**, 1735 (2006).

[25] S. Mehendale, M. Marathe, Y. Girard, V. Repain, C. Chacon, J. Lagoute, S. Rousset, and S. Narasimhan, Phys. Rev. B **84**, 195458 (2011).

[26] B. Yang, T. Muppidi, V. Ozoliņš, M. Asta, Phys. Rev. B **77**, 205408 (2008).

[27] E. D. Tober, R. C. F. Farrow, R. F. Marks, G. Witte, K. Kalki, and D. D. Chambliss, Phys. Rev. Lett. **81**, 1897 (1998).

[28] P. Giannozzi *et al.*, J. Phys.: Condens. Matter **21**, 395502 (2009).

[29] U. von Barth and L. Hedin, J. Phys. C: Solid State Phys. **5**, 1629 (1972).

[30] We have used the J. P. Perdew, K. Burke, and M. Ernzerhof form of [J. P. Perdew, K. Burke, and M. Ernzerhof, Phys. Rev. Lett. **77**, 3865 (1996)] for the Fe-Au/Ru(0001) or hexagonal configurations, and the Perdew-Wang form [J. P. Perdew and Y. Wang, Phys. Rev. B **45**, 13244 (1992)] for the Fe-Au/Mo(110) or centered rectangular configurations.

[31] H. J. Monkhorst and J. D. Pack, Phys. Rev. B **13**, 5188 (1976).

[32] M. Methfessel and A. T. Paxton, Phys. Rev. B **40**, 3616 (1989).

[33] M. Marathe, M. Imam, and S. Narasimhan, Phys. Rev. B **79**, 085413 (2009).

[34] M. Imam and S. Narasimhan, J. Magn. Magn. Mater. **323**, 1873 (2011).

[35] S. Blügel, Appl. Phys. A **63**, 595 (1996).

[36] J. M. Sanchez, F. Ducastelle, and D. Gratias, Physica A **128**, 334 (1984).

[37] J. M. Sanchez, Phys. Rev. B **48**, 14013 (1993).

[38] F. Cleri and V. Rosato, Phys. Rev. B **48**, 22 (1993).

[39] A. Díaz-Ortiz, F. Aguilera-Granja, K. Michaelian, E. O. Berlanga-Ramírez, J. M. Montejano-Carrizales, and A. Vega, Physica B **370**, 200 (2005).

[40] S. M. Foiles, Phys. Rev. B **32**, 7685 (1985).

[41] P. C. Kelires and J. Tersoff, Phys. Rev. Lett. **63**, 1164 (1989).

[42] K. Kawasaki, in *Phase Transitions and Critical Phenomena*, edited by C. Domb and M. S. Green (Academic Press, New York, 1972), Vol. 2, p. 465.

[43] B. Arnold, A. Díaz-Ortiz, G. L. W. Hart, and H. Dosch, Phys. Rev. B **81**, 094116 (2010).

[44] A. Díaz-Ortiz, H. Dosch, and R. Drautz, J. Phys.: Condens. Matter **19**, 406206 (2007).

[45] A. van der Walle and G. Ceder, J. Phase Equilib. **23**, 348 (2002).

[46] A. Díaz-Ortiz, R. Drautz, M. Fähnle, H. Dosch, and J. M. Sanchez, Phys. Rev. B **73**, 224208 (2006).

[47] A. Díaz-Ortiz and H. Dosch, Phys. Rev. B **76**, 012202 (2007).

[48] G. L. W. Hart and R. W. Forcade, Phys. Rev. B **77**, 224115 (2008).

[49] M. Marathe, M. Imam, and S. Narasimhan, Appl. Surf. Sci. **256**, 449 (2009).

[50] J.-P. Serre, *Cours d'Arithmetique* (Presses Universitaires de France, Paris, 1970).